Electronic Supplementary Material (ESI) for CrystEngComm.

Characterising the role of water in sildenafil citrate by NMR crystallography: Supplementary Information

Anuji Abraham, David C. Apperley, Stephen J. Byard, Andrew J. Ilott, Andrew J. Robbins, Vadim Zorin, Robin K. Harris and Paul Hodgkinson

Single crystal X-ray diffraction

Crystal data: $[C_{22}H_{31}N_6O_4S]^+$, $[C_6H_7O_7]^-$, $0.5H_2O$, M = 675.71 g mol^{-1}, orthorhombic, space group Pbca, a = 24.0290(10), b = 10.9805(5), c = 24.3497(10) Å, U = 6424.7(5) Å^3, F(000) = 2856, Z = 8, D_c = 1.397 mg m^{-3}, μ = 0.171 mm^{-1} (Mo-Kα, λ = 0.71073 Å), T = 120.0(2) K. 58096 reflections ($1.67 \leq \theta \leq 25.5°$) were collected on a Bruker SMART-CCD 6000 diffractometer (ω-scan, 0.3°/frame) yielding 5985 unique data (R_{merg} = 0.1325). The structure was solved by direct methods and refined by full-matrix least squares on F^2 for all data using SHELXTL software[1,2]. All non-hydrogen atoms were refined with anisotropic displacement parameters. H-atoms were located on the difference map and refined isotropically. Final w$R_2(F^2)$ = 0.1632 for all data (585 refined parameters), conventional R_1 (F) = 0.0524 for 3682 reflections with $I \geq 2\sigma$, GOF = 0.991.

Thermogravimetric analysis

TGA data was acquired on a Perkin Elmer Pyris 1 instrument, heating from ambient temperature to 200 °C at 10 °C min^{-1}. Raw data and plots can be found in data package for this publication.

Dynamic vapour sorption

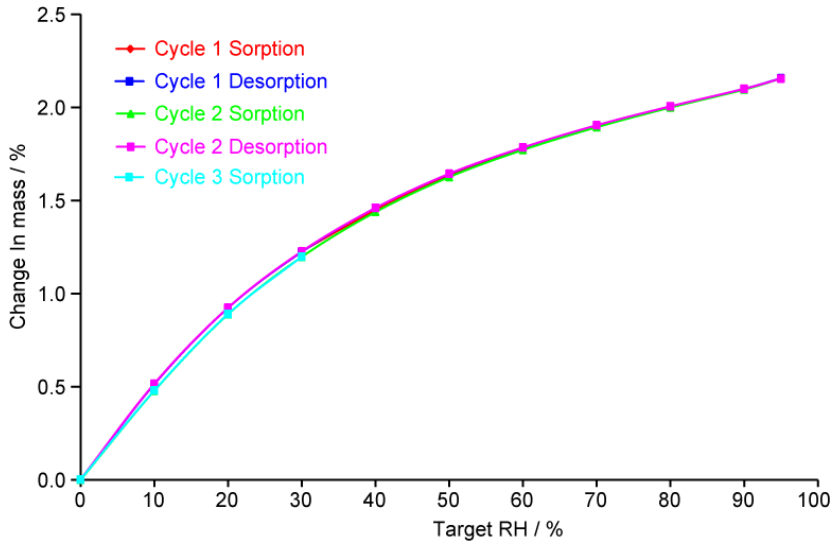

Figure S1: Dynamic vapour sorption isotherm for sildenafil citrate.

Dynamic vapour sorption isotherms were performed using a DVS-1 instrument supplied by Surface Measurement Systems (London, UK). Instrument performance checks were carried out using traceable standards of sodium chloride and lithium chloride. The RH cycle was taken from 30% to 95% to 0% to 30% at 25 °C. RH changes of 10% were used, except for the step between 90% and 95% RH. This cycle was completed twice for each sample. A target equilibrium condition of mass change less than 0.0002% per minute was used, with minimum

and maximum equilibrium periods of 10 and 360 min, respectively. 53 mg of sample was placed in a gauze basket, using nitrogen as the carrier gas at a flow rate of 100 mL/min. The results are shown in Figure S1. The two cycles are essentially identical, indicating that there are no induced crystallographic changes over the entire humidity range.

^{2}H NMR

Table S1: ^{2}H T_1 relaxation times

Site	–35 °C (warming)	+55 °C (warming)	+70 °C (cooling)
Water	37 ms		
~11 ppm	11.8 s	2.2 ± 0.1 s	3.7 ± 0.6 s
O33H	14.5 s	1.4 ± 0.6 s	(S/N too poor)

Figure S2 shows the fitting of the spectrum obtained at –58 °C to a quadrupolar spinning sideband manifold using gsim[3]/pNMRsim[4], using the parameters of Table S2. The feature around 11 ppm has been fitted as the sum of two components of equal intensity and line-shape but different chemical shifts in order to achieve a stable fitting. The resulting parameters have limited physical significance.

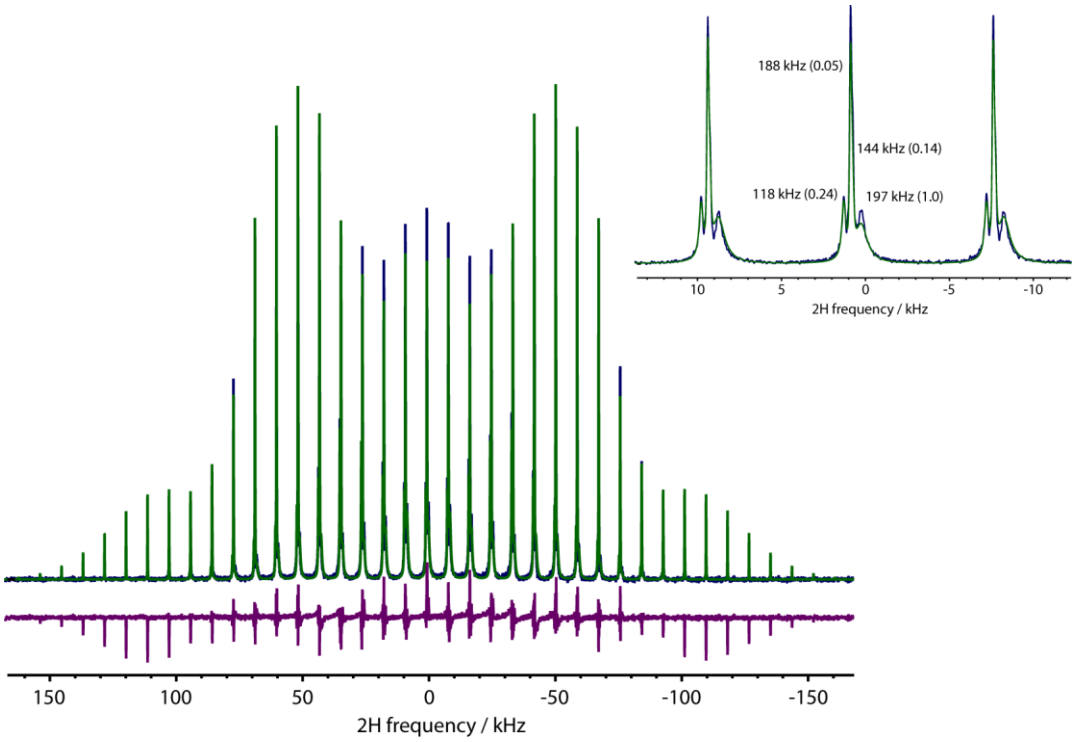

Figure S2. Fitting of ^{2}H MAS spectrum of the hydrated sample obtained at –58 °C. The inset around the centreband shows the fitted quadrupolar parameters, χ and asymmetry (in parentheses).

Table S2: Fitting parameters for ^{2}H MAS spectrum of hydrated sildenafil citrate at –58 °C

Assignment	O33H	2 × NH + 2 × citrate		Water
Shift / ppm	16.7	11.6	10.4	3.2
Linewidth / Hz	302	136	238	880
Intensity fraction	20%	51%		29%
C_Q / kHz	118	188	144	97
η	0.24	0.05	0.14	1
Gaussian fraction	10%	68%		0%

Table S3: Fitting parameters for ^{2}H MAS spectrum of dehydrated sildenafil citrate at –58 °C

Assignment	O33H	2 × NH + 2 × citrate
Shift / ppm	16.3	11.2
Linewidth / Hz	237	247
Intensity fraction	18%	82%
C_Q / kHz	121	167
η	0.12	0.22
Gaussian fraction	2%	20%

The quantitative analysis of the ^{2}H EXSY spectra is not straightforward due to the limited signal-to-noise ratio and significant overlap of the peaks at 10 and 11.5 ppm, creating a tension between integrating over the full volume of a peak to maximise sensitivity and reducing the quality of the integrals due to peak overlap. Simple integration of peak volumes failed to deliver robust results, and a hybrid method involving limited integration in the indirect dimension and peak fitting in the direct dimension was developed. The EXSY spectrum at the shortest (10 ms) mixing time was used to extract information on the lineshapes of the three resolved sites; the three rows containing the peak maxima were fitted to obtain the exact frequency, linewidth and lineshape (as a Lorentzian/Gaussian fraction) of the three resolved sites. Slices through the 2D spectrum centred on the three peak maxima in the indirect dimension were then integrated using N points to either side. These three slices were deconvoluted as a weighted sum of the lineshapes determined previously plus an overall baseline offset. Using the information on the lineshapes derived at short mixing time (when the diagonal peaks are well defined) means that only four parameters (three amplitudes plus a baseline) need to be fitted. This allowed the areas of the peaks to be determined robustly including in the limit where the peaks are barely distinguished from the background noise. Build-up / decay curves as a function of mixing time were then plotted for the nine peaks in the EXSY spectrum. The integration width parameter N was varied to find an appropriate trade-off between increasing signal-to-noise ratio and compromising the quality of the derived build-up curves.

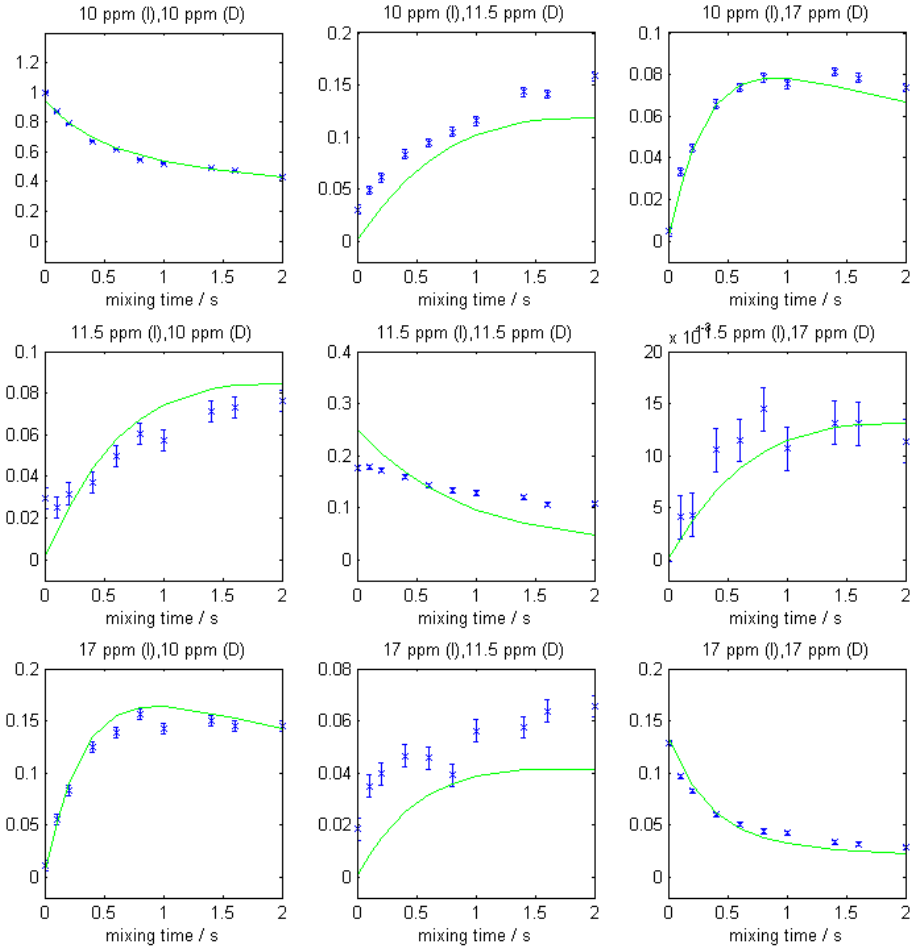

Figure S3. Fitting of ^{2}H DQ/SQ EXSY data obtained on a wet sample using cross-polarisation at ¬30 °C. (I) refers to the indirect (double-quantum) dimension, (D) to the direct (single-quantum) dimension.

Figures 4 and S3 show the fits of the resulting data to a model of three exchanging sites. The fitting parameters were: three amplitude parameters corresponding to the initial (zero mixing time) signal intensities, six rate constants for the forward / backward exchanges between the sites and three relaxation rates for the three sites. The fitted relaxation rates for two of the sites were zero within the fitting error and so could be fixed at zero without affecting the overall fit quality. A non-zero relaxation rate for the signal at 10 ppm was required for a satisfactory fit. Not least because cross-polarisation was used to create the initial magnetisation, the final equilibrium intensities could not be assumed to be proportional to the initial intensities, and so it was necessary to fit both forward and backward rates separately. The number of free parameters makes the fitting somewhat unstable. While the overall fit quality is reasonable considering the modest signal-to-noise ratio, some individual curves are not fitted particularly well. These systematic errors no doubt relate to features that are difficult to model, such as the known exchange between the water resonance (unobserved in these CP-based experiments) and the citrate resonance at 17 ppm, as well as the presence of multiple sites in the 10 ppm resonance. (Attempts to include a non-exchanging fraction of the 10 ppm signal resulted in much poorer fits). As a consequence, the physical significance of the fitted parameters and the statistical uncertainties reported in Table 1 is rather limited.

Table S4. Fitted kinetic parameters[a] (in s^{-1}) from ^{2}H DQ/SQ EXSY data acquired at (top) –30 °C and (bottom) –50 °C using cross-polarisation.

	10 ppm	11.5 ppm (O35H?)	17 ppm (O33H)
Intensity	65%	18%	17%
10 ppm	0.256 ± 0.006	0.70 ± 0.03 (0.33)	2.22 ± 0.04 (1.21)
11.5 ppm	0.153 ± 0.009	0	0.15 ± 0.03 (0.24)
O33H	0.66 ± 0.01	0.37 ± 0.03	0

	10 ppm	11.5 ppm (O35H?)	17 ppm (O33H)
Intensity	73%	16%	12%
10 ppm	0.348 ± 0.006	0.63 ± 0.04 (0.27)	2.20 ± 0.04 (1.18)
11.5 ppm	0.119 ± 0.008	0	0.00 ± 0.02 (–)
O33H	0.63 ± 0.01	0.35 ± 0.04	0

[a] Off-diagonal entries are rates of exchange between sites. Diagonal entries correspond to T_1 relaxation rates (10 ppm site only). Figures in parentheses are geometric means of the forward and backward rates between a pair of sites.

The fitted rate of relaxation of the 10 ppm peak from Table S4 is consistent with the measurements of the T_1 from saturation recovery experiments. The fact that the decay curves of the other sites can be fitted without including relaxation implies that the intrinsic rate of relaxation associated with these sites is low and their effective T_1 is determined by exchange with the other faster-relaxing sites. The figures in parenthesis in Table S4 are the geometrical averages of the forward and backward exchange rates between pairs of sites. These are expected to be more robust than the individual rates and can be used as a measure of the overall rate of magnetisation exchange between pairs of sites. Comparing the parameters obtained at the two study temperatures, only the relaxation rate parameter is temperature dependent as might be expected, but the exchange rates are either indistinguishable or differ erratically e.g. the effectively zero rate of exchange from the 11.5 to the 17 ppm resonance at –50 °C. This strongly suggests that the magnetisation exchange between the sites observed by cross-polarisation is dominated by spin-diffusion rather than chemical exchange. The data clearly shows much faster spin diffusion between the peak at 10 ppm and the citrate peak at 17 ppm than between other pairs of sites. This is consistent with an analysis of the distances between exchangeable H sites in the sildenafil citrate structure. O33H (17 ppm peak) is close at 2.65 Å (corresponding to a ^{2}H homonuclear dipolar coupling of 152 Hz) to the O31H (contained in the 10 ppm peak) but is some distance (4.67 Å, corresponding to a coupling of only 28 Hz) from O35H (contained in the 11.5 ppm peak). Instead, the C35 carboxylic acid H is closest to the potentially exchangeable H on N5 (3.82 Å, corresponding to a modest coupling of 51 Hz). The deuterium spin-diffusion is thus consistent with the assignments of the peaks, but the overlap of the sites makes it is difficult to draw further conclusions.

Peak assignment

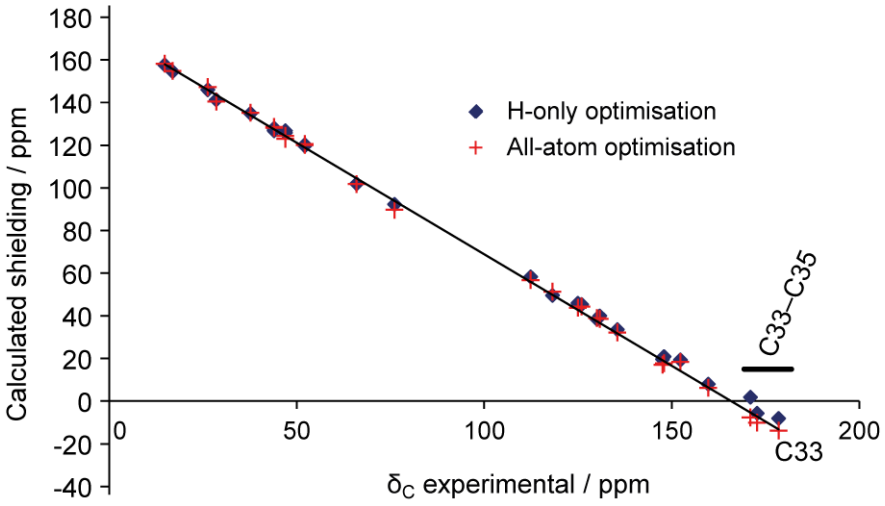

Figure S4: Correlation between calculated isotropic chemical shifts vs. the experimental shifts of hydrated sample at –80 °C with (blue diamonds) optimisation of the H-atoms only and (red cross) optimisation of all atoms prior to NMR calculation. The red line, from a linear regression to the all-atom data points, has gradient –1.046.

The CASTEP .magres files were processed by magres2pNMRsim to create tables of chemical shift (unreferenced) and quadrupolar information. The atomic labelling was added based on a PDB file from Materials Studio, which was assumed to order atoms of given type in the same way as the CASTEP output files. The labelling of the atoms was consistent with that of the original CIF, and can be safely assumed to be consistent between the different calculations. Viewing the PDB in Mercury allowed a mapping to be constructed between the labelling used in the calculations and the original labelling of Scheme 1, which is used for consistency with earlier work. Note that there are potential ambiguities in the mapping of carbons in the piperazine ring (C24/25 vs. C27/C28) and in the "orientation" of the citrate ion, but these are defined in the table below by the "crystallographic" labelling of the CIF. Methyl hydrogens were assumed to be in fast exchange and so their isotropic shifts were averaged and a single label used e.g. H13 for the three hydrogens attached to C13. The hydrogen labels were similarly remapped in terms of the molecular labelling of Scheme 1. Plots etc. were generated automatically in Matlab using this mapping, minimising the risks of mislabelling.

Table S5. Labelling and assignment of experimentally observed peaks[a] in sildenafil citrate

Crystallographic	*This work and Ref. 5*	*Chemical shift (wet) / ppm*	*Chemical shift (dry) / ppm*	*Assignment notes*[d]
C19	C1	147.6	147.0	L? H11: 2.1 Å
C15	C4	148.0[c]	148.2[c]	L? N5H: 2.1 Å
C14	C6	152.3[c]	152.2[c]	C, L? N5H: 2.1 Å
C17	C8	135.5	136.0	C, L? H11: 2.8 Å
C16	C9	125.0	124.5	C?, L? H10: 2.7 Å
C18	C10	37.7	37.4	C, S
C20	C11	28.6	26.7	S? H12: 2.2 Å
C21	C12	26.3	27.7	S? H11: 2.2 Å
C22	C13	14.8	16.0	C? H12: 2.2 Å
C8	C14	118.2	117.7	C, L H15: 2.1 Å, N5H: 2.6 Å
C7	C15	130.1	130.6	S
C6	C16	126.0	126.6	C?, M, L H17: 2.1 Å, H15: 2.2 Å
C11	C17	130.8	131.6	S H18: 2.1 Å
C10	C18	112.4	112.7	C, S H17: 2.2 Å
C9	C19	159.8	159.8	C, L H18: 2.2 Å, N5H: 2.5 Å, H30: 2.7 Å
C12	C20	66.0	66.4	C, S, L H21: 2.2 Å, H18: 2.5 Å
C13	C21	16.9	16.0	C? H20: 2.2 Å
C5	C22	43.8	44.3	L? N26H: 2.1 Å
C1	C24	44.7[b]	43.8/44.7[b]	H25: 2.2 Å
C2	C25	52.2[b]	52.6[b]	C, L? N26H: 2.1 Å, C25/H24: 2.1 Å, C27/H28: 2.1 Å
C3	C27			
C4	C28	44.7[b]	43.8/44.7[b]	C? H27: 2.1 Å
C26	C30	47.0[b]	47.1[b]	C?, S? O31H: 2.6 Å
C25	C31	76.1	76.0	C, S, L O31H: 2.0 Å, H30: 2.2 Å, H32: 2.2 Å
C24	C32	47.0[b]	47.4	C?, L? O33H: 2.5 Å, O31H: 2.6 Å
C23	C33	172.8	170.1	M, L O33H: 2.0 Å, H32: 2.1 Å
C28	C34	178.5	178.4	C, L O33H: 2.4 Å, O31H: 2.5 Å, H32: 2.7 Å, H30: 2.7 Å
C27	C35	171.0	171.2	M, S O31H: 2.0 Å, H30: 2.1 Å
1H18, 2H18, 3H18	H10	**4.9**	**4.9**	
1H20, 2H20	1H11, 2H11	**3.6**	**3.5**	
1H21, 2H21	1H12, 2H12	**2.4**	**2.5**	
1H22, 2H22, 3H22	H13	**2.1**	**2.5**	
H7	H15	**9.6**	**9.6**	
H11	H17	**7.9**	**7.6**	
H10	H18	**6.6**	**6.7**	
1H12, 2H12	1H20, 2H20	**4.9**	**5.0**	

1H13, 2H13, 3H13	H21	**2.6**	**2.5**	
H51, H52, H53	H22	**4.0**	**3.9**	
1H01	1H24	**3.7**[b]	**4.4**[b]	
2H01	2H24	**5.5**[b]		
H21, H22	1H25, 1H25	**4.4**[b]	**4.4**[b]	HETCOR for dry sample resolves peaks at 52.5 ppm/4.3 ppm and 52.9 ppm /4.4 ppm for $^{13}C/^{1}H$ shift.
H31, H32	1H27, 1H28			
H41	1H28	**3.7**[b]		
H42	2H28	**5.5**[b]		
1H26, 2H26	1H30, 2H30	**3.1**[b]	**3.0**	
1H24, 2H24	1H32, 2H32	**3.1**[b]	**3.2**	
H3N	N5H	11.8	11.6	From C19 cross-peak
H2N	N26H	10.8	10.9	From C25/C27 cross-peak
H7O	O31H	**10.3**	**10.7**	
H5O	O33H	17.1	16.4	From C33 cross-peak
H9O	O35H	11.6	12.1	From C35 cross-peak
H1W	1HW	Not observed. Included for mapping.		
H2W	2HW			
N1	N23			
N2	N26			
N3	N5			
N4	N7			
N5	N3			
N6	N2			

[a] ^{13}C shifts taken from CP/MAS spectrum acquired at 75.4 MHz and at –80 °C. ^{1}H shifts obtained from HETCOR experiments at 100.6 MHz; bold numbers indicate value obtained from experiment with short mixing-time, with remaining peaks taken from indicated correlation observed at the longer mixing time.

[b] The followings sets of resonances are heavily overlapped and are represented by single shift values corresponding to the peak maximum in the 1D ^{13}C spectrum (except in cases where multiple peaks could be resolved in the HETCOR): C24/C28, C30/C32 and C25/C27.

[c] ^{13}C shift values extracted from HETCOR spectra at 100.6 MHz (apparent shifts at 75.4 MHz are marginally affected by second-order quadrupolar effects).

[d] Symbols used to indicate basis of assignment: C – computed ^{13}C shift, S – "short range" cross-peak (visible at 100 μs mixing time), L – "long range" correlation peak, M – movement of peak position in wet vs. dry samples. A qualifying ? indicates that the evidence is suggestive rather than definitive. Distances to non-bonded H's up to a distance of 2.5 Å are shown. Some longer distances are included where these correspond to a potential cross-peak in Fig. 6.

Data bundle information

Table S6: Summary of data contained in associated data bundle.

Data bundle	Results presented	Comments
Sildenafil_citrate_AJR.zip	Figure 1	Varian .fid files containing 75 MHz ^{13}C spectra as a function of temperature: ajr19Mar0701.fid … ajr20Mar0714.fid
Sildenafil-citrate-HETCOR.zip	Figure 6	Varian .fid files containing $^{13}C/^{1}H$ HETCOR data (see contained README for details)
sildenafil-citrate-2HVT.tar	Figure 2	Spinsight files containing ^{2}H VT data (see contained README for further information)
sildenafil-citrate-2HEXSY.tar	Figures 3 & 4	Raw (Spinsight) and processed data for 2H DQ/SQ EXSY experiments (see contained README for further information)
sild13dvs0015.xls	Figure S1	Dynamic Vapour Sorption results (Excel spreadsheet)
SildenafilCitrateTGA.zip	(Not shown)	TGA results for "wet" and "dry" sample as Excel spreadsheets.

References

1. G. M. Sheldrick, *Acta Cryst., Sect. A,* **64** (2008) 112–122.

2. O. V. Dolomanov, L. J. Bourhis, R. J. Gildea, J. A. K. Howard and H. Puschmann, *J. Appl. Cryst.*, **42** (2009) 339–341.

3. V. Zorin, Gsim – a visualisation and processing program for solid-state NMR, URL: http://gsim.sourceforge.net.

4. P. Hodgkinson, pNMRsim: a general simulation program for large problems in solid-state NMR,URL: http://www.dur.ac.uk/paul.hodgkinson/pNMRsim.

5. D.C. Apperley, P.A. Basford, C.I. Dallman, R.K. Harris, M. Kinns, P.V. Marshall and A.G. Swanson, *J. Pharm. Sci.* **94** (2005) 516–523.